JOURNAL OF GEOPHYSICAL RESEARCH, VOL. 106, NO. C4, PAGES 7139–7155, APRIL 15, 2001

Influences of diurnal and intraseasonal forcing on mixed-layer and biological variability in the central Arabian Sea

Julian P. McCreary, Jr.,[1] Kevin E. Kohler,[2] Raleigh R. Hood,[3] Sharon Smith,[4] John Kindle,[5] Albert S. Fischer,[6] and Robert A. Weller[6]

Abstract. A three-dimensional, physical-biological model of the Indian Ocean is used to study the influences of diurnal and intraseasonal forcing on mixed-layer and biological variability in the central Arabian Sea, where a mooring was deployed and maintained from October 1994 to October 1995 by the Woods Hole Oceanographic Institution Upper Ocean Processes group. The physical model consists of four active layers overlying an inert deep ocean, namely, a surface mixed layer of thickness h_1, diurnal thermocline layer, seasonal thermocline, and main thermocline. The biological model consists of a set of advective-diffusive equations in each layer that determine nitrogen concentrations in four compartments: nutrients, phytoplankton, zooplankton, and detritus. Both monthly climatological and "daily" fields are used to force solutions, the latter being a blend of daily-averaged fields measured at the mooring site and other products that include intraseasonal forcing. Diurnal forcing is included by allowing the incoming solar radiation to have a daily cycle. In solutions forced by climatological fields, h_1 thickens steadily throughout both monsoons. When h_1 detrains at their ends, short-lived, intense blooms develop (the model's spring and fall blooms) owing to the increase in depth-averaged light intensity sensed by the phytoplankton in layer 1. In solutions forced by daily fields, h_1 thins in a series of events associated with monsoon break periods. As a result, the spring and fall blooms are split into a series of detrainment blooms, broadening them considerably. Diurnal forcing alters the mixed-layer and biological responses, among other things, by lengthening the time that h_1 is thick during the northeast monsoon, by strengthening the spring and fall blooms and delaying them by 3 weeks, and by intensifying phytoplankton levels during intermonsoon periods. Solutions are compared with the mixed-layer thickness, phytoplankton biomass, and phytoplankton production fields estimated from mooring observations. The solution driven by daily fields with diurnal forcing reproduces the observed fields most faithfully.

1. Introduction

From a physical perspective, the oceanic mixed layer is important because of its influence on surface currents, air-sea fluxes, and sea surface temperature (SST). From a biological perspective, it is crucial because mixed-layer entrainment and thickness are important determinants of the nutrient flux into the euphotic zone and the average light intensity experienced by the phytoplankton. The Arabian Sea provides an excellent test bed for studying these biophysical processes because the annual cycles of entrainment, mixed-layer thickness, and biological activity are extreme owing to the strong, annually reversing monsoon winds.

Arabian Sea biology and upper ocean physics were intensively studied from 1994 to 1996 during the Joint Global Ocean Flux Study (JGOFS) program. As part of that effort, a mooring was deployed and maintained in the central Arabian Sea at 15.5°N, 61.5°E from October 1994 to October 1995 by the Woods Hole Oceanographic Institution (WHOI) Upper Ocean Processes group, in collaboration with the Lamont-Doherty Earth Observatory and the University of California, Santa Barbara [*Weller et al.*, 1998]. Among other things, it measured near-surface ocean temperatures, surface

[1]International Pacific Research Center, University of Hawaii, Honolulu, Hawaii.
[2]Oceanographic Center, Nova Southeastern University, Dania, Florida.
[3]University of Maryland Center for Environmental Science, Cambridge, Maryland.
[4]Rosenstiel School of Marine and Atmospheric Science, Miami, Florida.
[5]Naval Research Laboratory, Stennis Space Center, Mississippi.
[6]Woods Hole Oceanographic Institution, Woods Hole, Massachusetts.

Paper number 2000JC900156.
0148-0227/01/2000JC900156$09.00

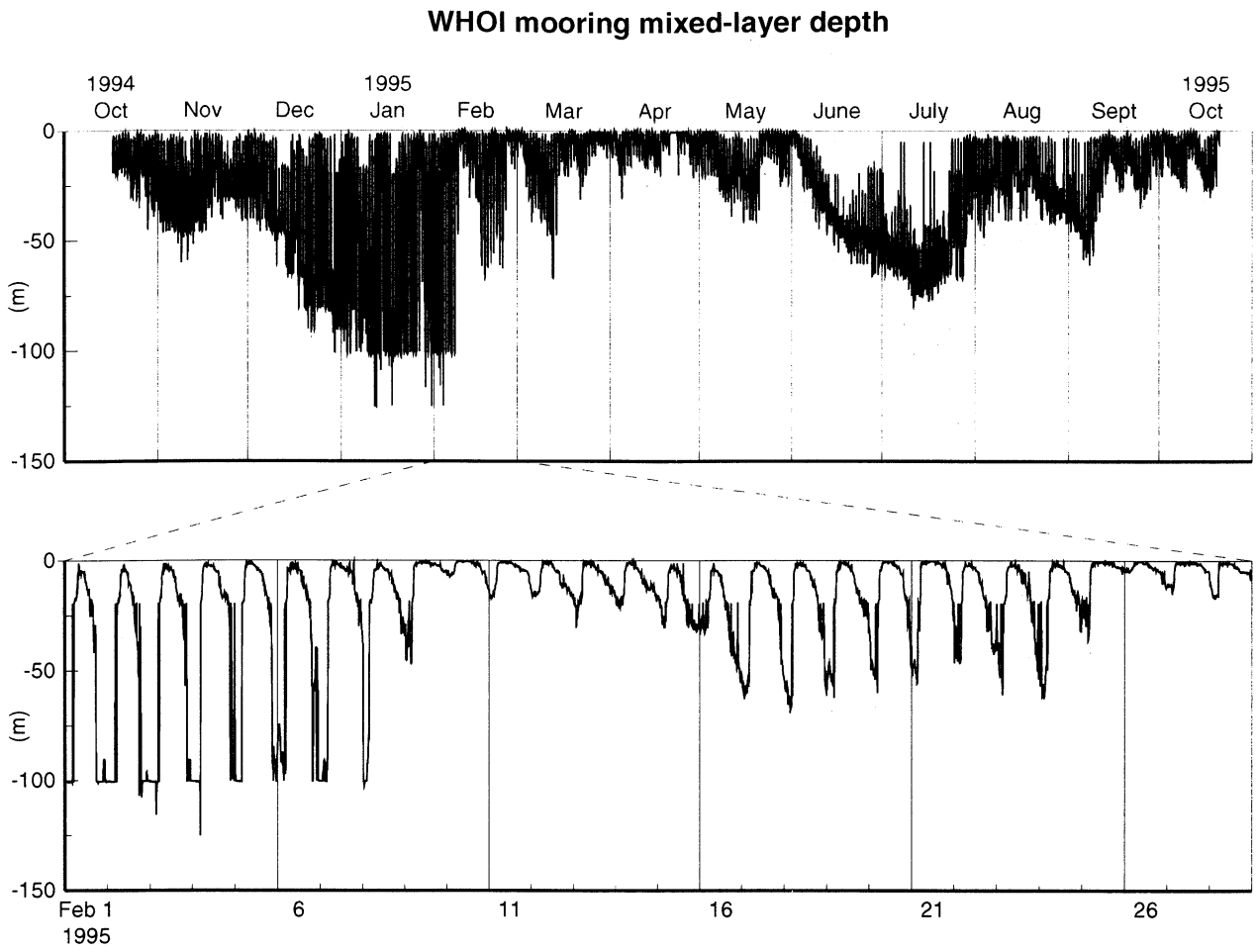

Figure 1. Time plots of mixed-layer thickness h_m estimated from temperature sensors on the WHOI mooring (top) for the entire year and during (bottom) February. The vertical resolution of the sensors increases with depth, from 5 m in the depth range -5 m $< z < -65$ m to 25 m for -100 m $< z < -250$ m. Data points are plotted every 15 min. Values of h_m are estimated by the depth at which temperature is 0.02°C cooler than the near-surface temperature at -0.43 m. Shading indicates typical times of the monsoon periods.

heat and buoyancy fluxes, and contained optical sensors from which phytoplankton biomass could be estimated. Figure 1 shows mixed-layer thickness h_m determined by the depth at which temperature was 0.02°C colder than SST. Prominent features are that h_m is thick twice a year during the southwest (June–September) and northeast (November–February) monsoons, that there are numerous pulses of thick (or thin) h_m of several weeks duration, and that the amplitude of the diurnal variability is large during the northeast monsoon but weaker during the southwest monsoon.

In a recent study, *McCreary et al.* [1996, hereinafter MKHO] coupled the physical model of *McCreary et al.* [1993, hereinafter MKM] to a four-component ecosystem model to examine the annual cycle of biological activity in the Arabian Sea. (Regrettably, serious errors were introduced into the text of MKM at the time of printing. An erratum can be found after page 248 of *Progress in Oceanography*, 1994, volume 33, number 3.) Their main run solution, which was forced by climatological winds, was able to reproduce all the major Arabian Sea phytoplankton blooms, a success due in part to the physical model's ability to simulate the annual cycle of h_m very well. Obvious deficiencies, however, were that their solution's spring and fall blooms were too intense and short-lived and that it lacked a summertime bloom (see the discussion of Figure 3 below).

In the MKHO solution, the mixed layer remained thick throughout the monsoon seasons. A possible biological cause of the aforementioned deficiencies, then, is simply that the phytoplankton in the MKHO model were not able to grow rapidly enough under low-light conditions. A possible physical cause is that the MKHO solution lacked natural intraseasonal variability. In contrast to climatological winds, the actual Arabian Sea monsoon winds have break periods that last for periods of a week or more. The mixed layer thins during these breaks (Figure 1), and blooms could occur provided it

thins sufficiently. Another possible physical cause is that the MKHO model lacked diurnal variability. With diurnal forcing, the mixed layer typically thins each day owing to surface heating (Figure 1), thereby increasing the depth-averaged light intensity sensed by the phytoplankton $\mathcal{I}$ and hence their growth rate. If this increase is large enough, phytoplankton growth could occur even though the daily maximum (or daily averaged) mixed-layer thickness is too large for blooms to develop.

In this paper, we use a coupled biological/physical model to investigate systematically effects due to diurnal and intraseasonal forcings and report the sensitivity of solutions to the specification of $\mathcal{I}$. Because of the high temporal resolution of the mooring data, we focus on understanding the causes of physical and biological variability in its vicinity. The coupled model is very similar to the MKHO system, differing mostly in aspects of its physical component. Solutions are forced by climatological and "daily" fields, the latter being a blend of daily averaged forcing fields measured at the buoy with other products, both with and without diurnal heating by the incoming solar radiation.

Among other things, we find that diurnal forcing affects solutions by altering the seasonal cycle of mixed-layer thickness, changing the daily averaged value of $\mathcal{I}$, and increasing vertical exchange between the mixed and subsurface layers (diurnal pumping); intraseasonal forcing is necessary for solutions to develop spring and fall blooms that are realistically broad. In addition, the solution driven by daily fields with diurnal forcing compares favorably with mixed-layer thickness and biological fields determined from the mooring data, suggesting that the model adequately represents fundamental physical and biological processes in the region.

2. The Coupled Model

2.1. The Physical Model

The physical model is a thermodynamic $4^1/_2$-layer system that extends throughout the Indian Ocean north of 29°S (Figure 2a). Dynamically, it is similar to the MKM model, differing in the addition of salinity, the inclusion of a diurnal thermocline layer (defined below), and several improvements of its mixed-layer physics. It is a modification of the *Han* [1999] (see [*Han et al.*, 1999]) model to include the diurnal thermocline layer. Here then we only discuss aspects of the physical model that are important for understanding the biological response. Specifically, we describe its layer structure and define the across-interface velocities that specify how water transfers from one layer to another in the surface region.

2.1.1. Layer structure. Figure 2b illustrates the layer structure of the model. It consists of four upper ocean layers with velocities $\mathbf{v}_i = (u_i, v_i)$, layer thicknesses h_i, temperatures T_i, and salinities S_i ($i = 1, 2, 3, 4$ is a layer index), overlying a deep inert ocean

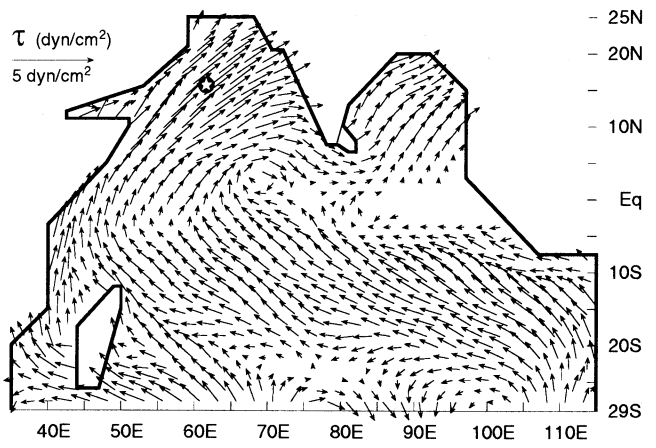

Figure 2a. A schematic diagram, showing the model domain and the winds that force the model on July 15, 1995 (see section 2.3). The star indicates the location of the WHOI mooring.

with temperature $T_d = 3°\mathrm{C}$ and salinity $S_d = 34.8$ practical salinity units (psu). The density of each layer is

$$\rho_i = \rho_0 \left(1 + \alpha_t T_i + \alpha_s S_i\right), \tag{1}$$

where $\rho_0 = 1\ \mathrm{g/cm^3}$, and $\alpha_t = -2.5 \times 10^{-4}\ °\mathrm{C}^{-1}$ and $\alpha_s = 8 \times 10^{-4}\ \mathrm{psu}^{-1}$ are thermal and salinity expansion coefficients. The layers correspond to either distinct oceanic regions or water mass types, namely, the surface mixed layer (layer 1), the diurnal thermocline (layer 2), the seasonal thermocline (layer 3; MKM's "fossil" layer), and the main thermocline (layer 4). The diurnal thermocline layer represents the region left behind when the mixed layer thins from its nighttime maximum to its daytime minimum; it allows the system to "remember" physical and biological variables when the mixed layer thins and so helps to prevent spurious vertical mixing between the mixed layer and the deeper ocean (see section 3.1.3.2). Fluid is allowed to transfer between the layers with velocities w_1, w_2, and w_3, and the system is thermodynamically active in that T_i, S_i, and ρ_i vary horizontally in response to surface heat and buoyancy fluxes, horizontal advection, entrainment, and detrainment. Finally, h_1, h_2, and h_3 are not allowed to become thinner than minimum values $h_{1\min} = 10$ m, $h_{2\min} = 1$ m, and $h_{3\min} = 10$ m. These minima are necessary to keep the model numerically stable, and solutions are not sensitive to their values provided they are sufficiently small.

As in the MKM model, layers 1 and 2 are thermodynamically independent in that h_i, S_i, and T_i are calculated separately, but dynamically they behave like a single layer with a density $\bar{\rho} = (h_1\rho_1 + h_2\rho_2)/(h_1 + h_2)$ and no velocity shear (i.e., $\mathbf{v}_1 = \mathbf{v}_2$). Thus the system can be described as being a $3^1/_2$-layer model (i.e., layers 1 + 2, layer 3 and layer 4) with an imbedded mixed layer (layer 1).

2.1.2. Across-interface velocities. The across-

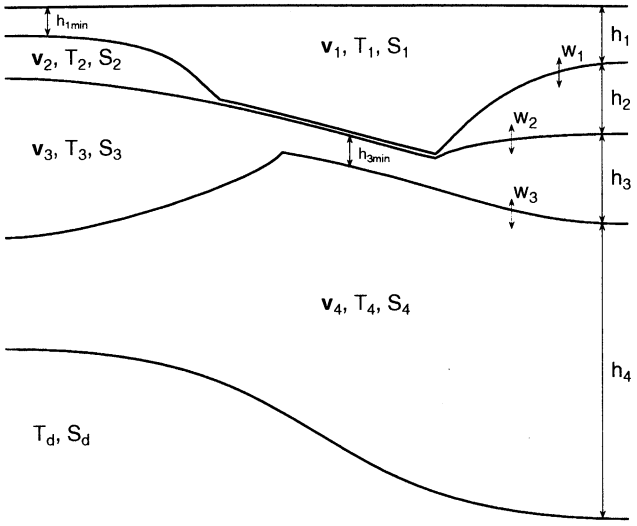

Figure 2b. Schematic diagram, illustrating the layer structure of the physical model.

interface velocities are a crucial part of the physical model, as they represent its vertical mixing processes. For the surface mixed region (layers 1 and 2), the velocities are

$$w_1 = w_k + w_{1c}, \tag{2a}$$

$$w_2 = w_d + w_r + w_{2c}. \tag{2b}$$

The key process in these equations is w_k, which specifies the entrainment into, and detrainment from, the mixed layer. It is determined by *Kraus and Turner* [1967] physics according to

$$w_k = \begin{cases} \dfrac{P_r}{\frac{1}{2}gh_1\Delta\rho'}, & P_r > 0 \\ \dfrac{h_{\rm mo} - h_1^-}{2\Delta t}, & P_r \le 0, \end{cases} \tag{3a}$$

where

$$P_r = mu_*^3 - \tfrac{1}{2}gh_1[-\alpha_t Q_1 + \alpha_s(\mathcal{R} - \mathcal{E})S_1] \tag{3b}$$

is the production of turbulent kinetic energy,

$$\Delta\rho' = \begin{cases} \rho_2 - \rho_1 + \delta\rho, & h_2 > 0 \\ \rho_3 - \rho_1, & h_2 = h_{2\rm min},\ h_3 > h_{3\rm min} \\ \rho_4' - \rho_1, & h_2 = h_{2\rm min},\ h_3 = h_{3\rm min} \end{cases} \tag{3c}$$

is the density jump at the base of the mixed layer, and

$$h_{\rm mo} = \frac{mu_*^3}{\frac{1}{2}g[-\alpha_t Q_1 + \alpha_s(\mathcal{R} - \mathcal{E})S_1]} \tag{3d}$$

is the Monin-Obukhov depth. In these equations, h_1^- is the layer 1 thickness at the previous time level, Δt is the model time step, Q_1 is the net surface heating in layer 1, $\mathcal{R} - \mathcal{E}$ is precipitation minus evaporation, mu_*^3 ($\equiv \mathcal{W}$) measures the generation of turbulence caused by wind stirring, u_* is the oceanic friction velocity, $m = 1$ is the wind-stirring coefficient, and $g = 980$ cm/s^2 is the acceleration of gravity. The term $\delta\rho = 2.5 \times 10^{-7}$ g/cm^3 is included in (3c) only to ensure that the denominator of (3a) never vanishes, and it otherwise does not influence the solution.

According to (3a), layer 1 entrains water when $P_r > 0$, and it detrains instantly (i.e., in one time step of the integration) to the Monin-Obukhov depth $h_{\rm mo}$ when $P_r \le 0$. According to (3c), it entrains water from the first layer beneath it that is not at its minimum thickness. Note that water of density ρ_4' is entrained from layer 4; it is specified as by *Han et al.* [1999] and is representative of a density value near the top of the main pycnocline (that is, ρ_4' is somewhat less than ρ_4).

As defined in section 2.1.1, the diurnal thermocline layer should reach its minimum thickness each day when h_1 attains its nighttime maximum. To ensure that this condition holds generally, w_2 includes the detrainment term,

$$w_d = -\frac{h_1 + h_2 - \hat{h}_1' - h_{2\rm min}}{t_d}, \tag{4a}$$

where

$$\hat{h}_1'(t') = \max(h_1), \qquad t_1 - t_{\rm day} < t' \le t_1, \tag{4b}$$

$t_1 = {\rm int}[(t - t_o)/t_{\rm day}]\, t_{\rm day} + t_o$, t is the time of integration, int(x) is the integer part of x, $t_{\rm day}$ is the length of a day, and $t_o = 0700$. Typically, t_o is the time just before the mixed layer begins to thin during the day (see Figures 4b and 7b). According to (4a), w_d adjusts h_2 until $h_1 + h_2$ has its maximum thickness attained during the previous day in a timescale of t_d. With this choice for w_d, h_2 fails to reach $h_{2\rm min}$ only when layer 1 detrains rapidly at the end of the monsoons and during break periods. At such times, we interpret layer 2 to be an upper part of the seasonal thermocline, one that is gradually mixed (absorbed) into the main seasonal thermocline with a timescale t_d.

Velocity w_r is an entrainment term ($w_r \ge 0$), which ensures that $h_1 + h_2$ is large enough for the bulk Richardson number of layer 1 to be greater than or equal to 0.4; it is needed only to keep the solution numerically stable along the Somali coast when the current becomes so strong during the southwest monsoon. Terms w_{1c} and w_{2c} are entrainment terms that ensure that h_1 and h_2 never become less than $h_{1\rm min}$ and $h_{2\rm min}$, respectively.

2.2. The Biological Model

The biological model consists of a set of advective-diffusive equations in each layer that determine the nitrogen concentrations in four compartments: nutrients N, phytoplankton P, zooplankton Z, and detritus D. Hyperbolic saturation functions are used to describe how the autotrophic production rate is related to photosynthetically active radiation (PAR) and nutrient concentration and how zooplankton growth is related to

food supply. Zooplankton mortality is included as a self-predation term (proportional to Z^2). The microbial loop is represented as a linear, remineralization pathway from D to N with the rate varying in proportion to D. Model equations and all but one of the parameters (the exception being I_o defined next) are the same as those of the MKHO system. The biological model is coupled to the physical model via the latter's $\mathbf{v}_i$, w_i, and h_i fields. Conversely, the physical model is influenced by the biological response through the effect of P on the absorption of penetrating radiation (see section 2.3).

The phytoplankton growth rate in each layer is given by $g_p \mathcal{I}_i \mathcal{N}_i$, where $g_p = 2.5$ day^{-1},

$$\mathcal{I}_i = \frac{1}{h_i} \int_{z_i}^{z_{i-1}} \frac{I(z)}{\sqrt{I^2(z) + I_o^2}}\, dz \tag{5}$$

is the phytoplankton light response function,

$$\mathcal{N}_i = \frac{N_i}{N_i + N_o} \tag{6}$$

is the nutrient response function, $\mathcal{I}(z)$ is PAR, $z_i = -\sum_{j=1}^{i} h_j$, and I_o and $N_o = 1$ μmol N/kg are half-saturation constants. Note that both $\mathcal{I}_i$ and $\mathcal{N}_i$ have maximum values of 1. For most solutions, $I_o = 40$ W/m^2, lower than the value of 100 W/m^2 used by MKHO. This change allows phytoplankton to grow under lower light conditions than they did in the MKHO model. We carried out a suite of test solutions to determine the "best" value for I_o, eventually choosing 40 W/m^2 because it produced biomass and productivity responses that compared best with estimates from the mooring data (see section 3.3). This value is appropriate for the low light-adapted phytoplankton communities present when h_1 is thick during the monsoons, but is rather low for the high light-adapted communities present during the intermonsoons (J. Marra, private communication, 1999).

This system is considerably simpler than many of the more sophisticated, ecosystem models currently used in biogeochemical studies [e.g., *Fasham et al.*, 1990; *Leonard et al.*, 1999]. We use it because our goal is to understand basic interactions between biology and physics rather than to simulate ecological complexity, and the simplicity of the $NPZD$ model allows these interactions to be more readily identified.

2.3. Forcing

The climatological wind stress, $\boldsymbol{\tau} = \rho_a C_D |\mathbf{V}| \mathbf{V}$, used to force the model is determined from Florida State University monthly mean pseudostress $|\mathbf{V}|\mathbf{V}$ averaged from 1970 to 1996 [*Legler et al.*, 1989], with $\rho_a = 0.001175$ g/cm^3 and $C_D = 0.0015$. Climatological heat fluxes are determined from monthly mean fields of air temperature T_a, specific humidity, net incoming solar radiation Q_r, outgoing long-wave radiation, and scalar wind $w_{\rm sc}$ derived by *Rao et al.* [1989, 1991]. They are obtained from standard bulk formulae by using model SST (T_1) in the calculation for the sensible and latent heat fluxes [*McCreary and Kundu*, 1989; MKM]. Precipitation $\mathcal{R}$ is provided by *Legates and Willmott* [1990].

"Daily" forcing from April 1993 through October 1995 consists of daily mean Fleet Numerical Meteorology and Oceanography Center $\boldsymbol{\tau}$ and 10-m scalar wind $w_{\rm sc}$ fields, as well as daily mean heat fluxes interpolated from the monthly climatological T_a, q_a, and Q_r fields described in the preceding paragraph. In addition, from October 16, 1994, to October 20, 1995, daily mean data from the WHOI mooring (15.5°N, 61.5°E) are blended into these forcing fields by using a Gaussian taper with an e-folding scale of 500 km, such that the forcing is composed entirely of buoy fields at the mooring site.

The oceanic friction velocity u_* in (3b) is determined from $w_{\rm sc}$ according to $u_* = \gamma^{\frac{1}{3}} \sqrt{C_D'(\rho_a/\rho_0)} w_{\rm sc}$, where $C_D' = 0.0014$, $\gamma(w_{\rm sc}) = 1 + [1 - (w_{\rm sc}/w_{\rm cr})^3]\theta(w_{\rm cr} - w_{\rm sc})$, θ is a step function, and $w_{\rm cr} = 5$ m/s. Coefficient γ is a factor that strengthens u^* at low wind speeds. We estimated its form by using wind data from the mooring [*Weller et al.*, 1998].

The incoming solar radiation Q_r is represented as the sum of penetrating and nonpenetrating parts according to

$$Q(z) = \phi Q_r e^{kz} + (1 - \phi) Q_r e^{k'z}, \tag{7}$$

where $k' \gg 0.1$ m^{-1}, $k = k_o + k_p P$, $k_o = 0.03$ m^{-1}, $k_p = 0.0381$ m^{-1}(μmol N/kg)$^{-1}$, and $\phi = 0.4$ is the fraction of Q_r that penetrates into the deeper ocean. This simple form for Q is based on a somewhat more complicated expression, found in the work of *Morel and Antoine* [1994] (also see *Price et al.* [1986] and *Paulson and Simpson* [1977]). According to (7), the solar radiation that is absorbed in layer 1, and hence that contributes to Q_1 in equation (3b), is $Q(0) - Q(-h_1)$. The PAR field is just the penetrating part of Q.

Diurnal forcing is included by allowing Q_r to go through a diurnal cycle as follows. Let $\overline{Q_r}$ be the daily-averaged net solar radiation. Then the diurnal cycle of Q_r is taken to be

$$Q_r(t') = \begin{cases} \pi \overline{Q_r} \cos(2\pi t'/t_{\rm day}), & 6 < t' < 18 \\ 0, & \text{otherwise,} \end{cases} \tag{8}$$

where $t' = \mathrm{mod}(t, t_{\rm day})$, and the units of t' and $t_{\rm day}$ are hours. For solutions without diurnal forcing, Q_r is obtained by linearly interpolating between adjacent values of $\overline{Q_r}$.

2.4. Numerics

Because of diurnal forcing, changes in h_1 and h_2 can be large in a single time step. To ensure numerical stability, we integrate the layer 1 and layer 2 equations for temperature, salinity, and the biological variables semi-implicitly. This is accomplished by writing the equations in finite difference form and then replacing variables at the central time step and location q_{ij} with their counterparts at the forward time step q_{ij}^+.

Another problem associated with diurnal forcing is that w_k becomes very large near the end of nighttime cooling events when $\Delta\rho' = \rho_2 - \rho_1 + \delta\rho$ becomes small. These large entrainment rates are eliminated either by daytime warming or by h_2 thinning to $h_{2\,\min}$ so that, according to (3b), $\Delta\rho'$ switches to the larger value $\rho_3 - \rho_1$. In the latter situation, there is considerable spurious entrainment if the switch is applied at the end of each time step, resulting in a mixed-layer depth that is too large. To avoid this problem, we calculate the precise time that $h_2 = h_{2\min}$ and thereby allow the switch to occur within each time step. (A similar technique is used to allow the switch to $\Delta\rho' = \rho_4' - \rho_1$ within a time step if necessary.)

Solutions are obtained on a C-grid of dimension $\Delta x = \Delta y = 55$ km and are integrated forward in time with a time step $\Delta t = 0.5$ hour. Boundary conditions are the same as in MKM. Initial values for temperature are T_1 = observed SST from *Rao et al.* [1989, 1991], $T_2 = T_\epsilon + 1°\mathrm{C}$, $T_3 = T_\epsilon$, where T_ϵ is defined by *Han et al.* [1999], and $T_4 = 15°\mathrm{C}$. Initial values for salinity are $S_1 = S_2$ = observed sea surface salinity from *Levitus et al.* [1994] data and $S_3 = S_4 = 35.4$ psu, and for layer thicknesses are $h_1 = 10$ m, $h_2 = 20$ m, $h_3 = 35$ m, and $h_4 = 300$ m.

The physical model is spun up from a state of rest for a period of 5 years beginning on April 15 by using climatological forcing. Then for the climatological solutions the coupled system is integrated for an additional $5\frac{1}{2}$ years, and the climatological plots shown in section 3.1 are taken from the last year of their respective solutions. For the daily solutions, we assume that the end of the uncoupled spin-up period is April 15, 1993. The coupled system is then integrated until November 1, 1995, by using daily winds, and the plots shown in section 3.2 are for the period from October 1, 1994, to November 1, 1995.

3. Results

Here, we report a series of solutions designed to isolate the influences of phytoplankton light sensitivity and of diurnal and intraseasonal forcing. In section 3.1, we discuss solutions driven by climatological forcing fields, which because of their simplicity more clearly illustrate basic processes. Then, in section 3.2 we report solutions driven by daily forcing fields, which illustrate influences of intraseasonal forcing. Finally, in section 3.3 we compare our most realistic solution to observed mixed-layer thickness, biomass, and production fields estimated from mooring data.

3.1. Climatological Forcing

3.1.1. Solutions without diurnal forcing. Figure 3 shows time series of biological variables and layer thicknesses at the mooring location (61.5°E, 15.5°N) for solutions forced by climatological fields without diurnal forcing, illustrating the responses when $I_o = 100$ W/m^2 (solution 1, top panel) and $I_o = 40$ W/m^2 (solution 2, middle and bottom panels). (Note the difference in scale of the vertical axes for solutions 1 and 2.) Solution 1 is the only solution reported with $I_o = 100$ W/m^2, all others having $I_o = 40$ W/m^2. It provides a link to the MKHO main run solution (their Figure 4), which also used $I_o = 100$ W/m^2; the minor differences between solution 1 and the MKHO main run are therefore all due to differences in the physical models.

Because the h_i fields of the two solutions are so similar, only layer thicknesses for solution 2 are shown in Figure 3. (The only visual difference between them is that h_1 is 10–15 m thinner for solution 1 at the times of the intense P_1 peaks in late February and September, owing to the feedback of P_i onto k.) At the beginning of the southwest monsoon in mid-May, h_1 begins to deepen due to entrainment w_k induced primarily by wind stirring $\mathcal{W}$. It continues to thicken until the end of August, when detrainment due to weaker winds and warming at the end of the southwest monsoon thins h_1 to the Monin-Obukhov depth h_{mo}. During the northeast monsoon, there is another cycle of thicker h_1, in this case due to entrainment caused primarily by surface cooling ($Q_1 < 0$). It ends in the spring when h_1 detrains to h_{mo} owing to surface heating.

In contrast to the h_1 fields, the biological variables differ considerably between the two solutions. In solution 1, entrainment mixes large layer 3 nutrient concentrations N_3 into layer 1 during both monsoons, and as a result N_1 increases continuously throughout the winter and summer, eventually attaining unrealistically high levels ($\sim$12 μmol N/kg during the southwest monsoon as compared with observed values of $\sim$4 μmol N/kg [*Morrison et al.*, 1998]). In response to the initial entrainment, P_1 develops blooms that peak in early November and June. These "entrainment" blooms, however, are short-lived despite the high nutrient levels because the entrainment continues to thicken h_1, thereby reducing the depth-averaged light intensity sensed by the phytoplankton in layer 1, $\mathcal{I}_1$, and hence their growth rate $g_p\mathcal{I}_1\mathcal{N}_1$. Consequently, strong blooms do not occur until h_1 detrains at the end of the monsoons. These spring and fall "detrainment" blooms are intense because of the buildup of high N_1 levels during summer and short-lived because of grazing by Z_1 and the rapid depletion of N_1 (see sections 3.5 and 3.8 of MKHO). As was discussed by MKHO, they are too intense, too brief, and delayed by at least a month in comparison with the blooms determined from Coastal Zone Color Scanner (CZCS) imagery and historical observations [*Banse*, 1987, 1994; *Banse and English*, 2000] and from measurements at the WHOI mooring (section 3.3 [*Dickey et al.*, 1998; *Marra et al.*, 1998]). Finally, note that there is a weak bloom during March. It is a weak secondary peak of a damped oscillation of the biological model excited by the intense spring bloom (see sections 3.5 and 4.3.2 of MKHO). There is also such a peak after the fall bloom that overlaps the November entrainment bloom.

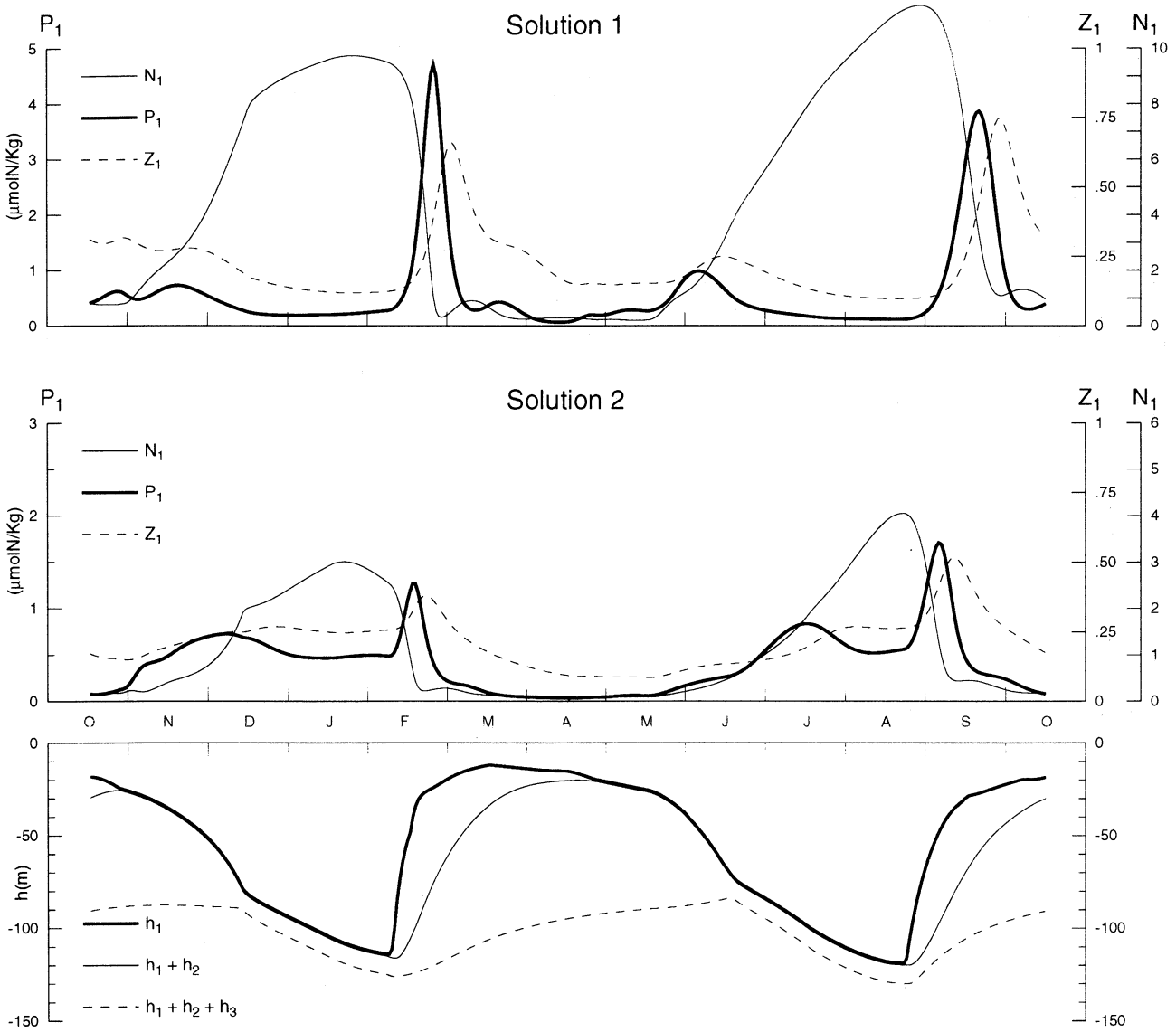

Figure 3. Time plots of layer thicknesses and biological variables for solutions forced by climatological fields without diurnal forcing, (top) when $I_o = 100$ W/m^2 (solution 1) and (middle and bottom) when $I_o = 40$ W/m^2 (solution 2). Note the difference in scale of the vertical axes between solutions 1 and 2. (bottom) Layer thicknesses h_1 (thick line), $h_1 + h_2$ (thin line), and $h_1 + h_2 + h_3$ (dashed line) are plotted below the time axis. P_1 (thick line), N_1 (thin line), and Z_1 (dashed line) concentrations are plotted above the axis in the top and middle panels. Shading indicates typical times of the monsoon periods.

In solution 2, P_1 levels are significantly larger during the monsoons when h_1 is thick because the phytoplankton are able to grow more rapidly under lower-light conditions. As a result of this sustained productivity, N_1 levels during the monsoons decrease to realistic values [*Morrison et al.*, 1998], and the spring and fall blooms are weaker, since the nutrient pool available to them is so much smaller. In addition, the spring and fall blooms start about 2 weeks earlier, because the phytoplankton respond more quickly to the initial decrease in h_1. Note also that the entrainment blooms, which in solution 1 are confined to the onsets of the monsoons before h_1 becomes too large, strengthen more gradually and last longer. This difference is likely due to N_2 being smaller in solution 2 because of greater P_2 growth; consequently, the onset of entrainment does not increase N_1 as rapidly and so P_1 grows more gradually. Similarly, there are no secondary oscillations after the spring and fall blooms, likely because N_2 entrainment is weak (or absent) and hence N_1 cannot increase enough to allow phytoplankton growth.

3.1.2. Solution with diurnal forcing. Figure 4a shows the climatological solution when diurnal forcing (8) is included (solution 3). In this case, two curves

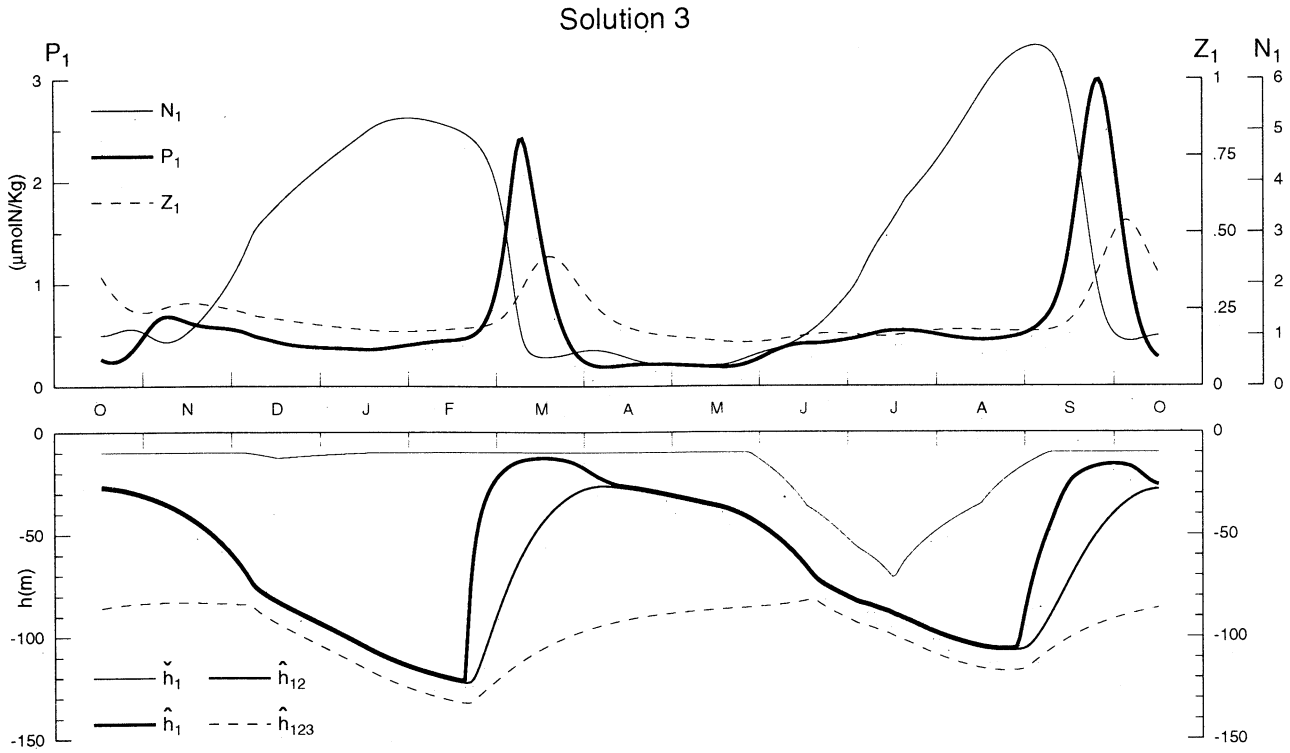

Figure 4a. As in the bottom panel of Figure 3, except for the solution forced by climatological fields with diurnal forcing (solution 3). There are two curves for h_1, indicating its maximum value $\hat{h}_1$ (thick line) and minimum value $\check{h}_1$ (thin line) on any given day. Curves $\hat{h}_{12}$ and $\hat{h}_{123}$ are the maximum daily values of $h_1 + h_2$ and $h_1 + h_2 + h_3$, respectively. Curves for the biological variables are their daily-averaged values. The spring and fall blooms are somewhat broader, more intense, and occur several weeks later than they do in solution 2 (Figure 3).

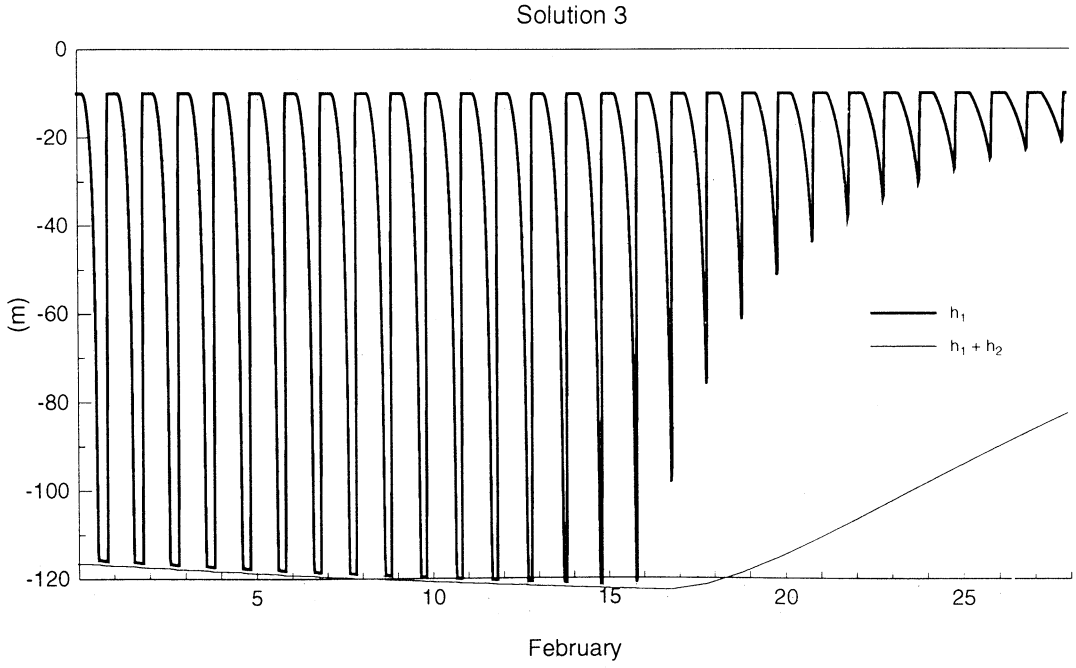

Figure 4b. Time plots of layer thicknesses for solution 3, showing instantaneous values of h_1 (thick curve) and $h_1 + h_2$ (thin curve) during February. The curves illustrate the layer structures for type 1 ($\check{h}_2 > h_{2\min}$) and type 2 ($\check{h}_2 = h_{2\min}$) diurnal pumping in the right-hand and left-hand portions of the figure, respectively.

are plotted for h_1 to indicate its diurnal cycle: its daily maximum $\hat{h}_1$ (thick curve) and minimum $\check{h}_1$ (thin curve) values. In addition, Figure 4b illustrates the diurnal cycle in detail for the month of February, plotting instantaneous values of h_1 and $h_1 + h_2$.

Diurnal variability of h_1 is caused by the daily sign reversal of Q_1. In solution 3, the reversal also always causes P_r to change sign, so that according to (2a) h_1 entrains every night and adjusts to $h_{\rm mo}$ (or $h_{1\rm min}$) every day. Typically, the solution develops its maximum possible diurnal cycle, with h_1 thinning to its minimum thickness $h_{1\rm min} = 10$ m. This happens because wind stirring is weak enough during most of the year that $h_{\rm mo} < h_{1\rm min}$. The only time the diurnal amplitude weakens appreciably is during the southwest monsoon when $\mathcal{W}$ is large and $h_{\rm mo} > h_{1\rm min}$.

Overall, the annual cycles of physical and biological variables are similar in Solutions 2 and 3, but there are notable differences between them. In comparison with the h_1 field of solution 2, for example, $\hat{h}_1$ is 10–15 m thicker throughout much of the intermonsoon periods, it thins about 2 weeks later at the end of the northeast monsoon, and is 10–15 m thinner than h_1 during August. Because the mixed-layer response in each case is determined in such dynamically different ways, it is not clear just what aspects of diurnal cycling cause these differences: In solution 2, h_1 either entrains steadily (throughout the monsoons) or remains at the Monin-Obukhov depth $h_{\rm mo}$ or $h_{1\rm min}$ (during the intermonsoon periods), whereas in solution 3 layer 1 entrains and detrains each day and $\hat{h}_1$ never adjusts to $h_{\rm mo}$.

In comparison with the phytoplankton response in solution 2, the spring and fall blooms in solution 3 are broader, stronger, and delayed about 3 weeks, and P_1 levels are somewhat lower during the monsoons and significantly higher during the spring intermonsoon. In addition, N_1 levels are higher throughout the entire annual cycle, especially near the end of the monsoons. Some of these differences are traceable to changes in the annual mixed-layer response: The delay in the spring-bloom onset results partly from $\hat{h}_1$ thinning later at the end of the northeast monsoon, and the larger N_1 levels happen partly because the periods of deep $\hat{h}_1$ are longer. Other differences likely result from the diurnal pumping processes discussed next.

3.1.3. Diurnal processes. There are two basic diurnal processes at work in the model: modification of the depth-averaged light intensity sensed by the phytoplankton $\mathcal{I}_1$ and enhanced vertical mixing between the mixed and subsurface layers. To help illustrate the influence of these processes on the phytoplankton growth rate, Figure 5 plots $\overline{\mathcal{I}_1}$, $\overline{\mathcal{N}_1}$, and $\overline{\mathcal{I}_1\mathcal{N}_1}$ for solution 2 (top panel) and solution 3 (bottom panel), the overbars indicating daily averages.

3.1.3.1. Modification of $\overline{\mathcal{I}_1}$: A comparison of $\overline{\mathcal{I}_1}$ curves in Figure 5 shows that $\overline{\mathcal{I}_1}$ is larger in solu-

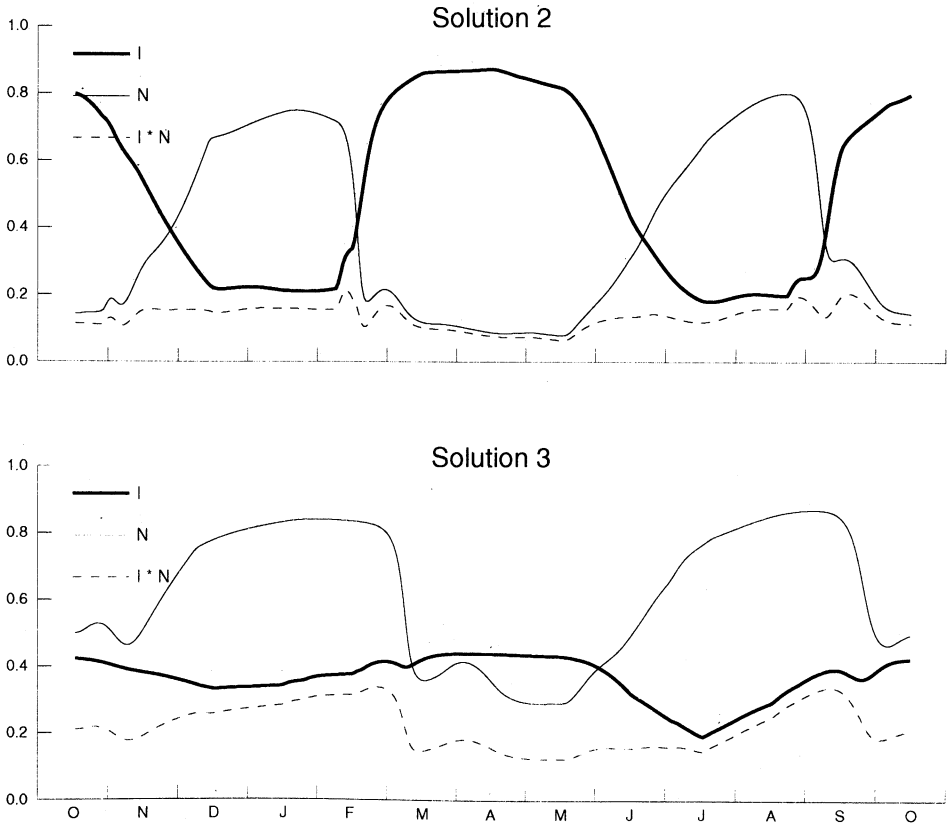

Figure 5. Time plots of $\mathcal{I}_1$, $\mathcal{N}_1$, and $\mathcal{I}_1\mathcal{N}_1$ for (top) solution 2 and daily averages of those quantities for (bottom) solution 3. Shading indicates typical times of the monsoon periods.

tion 3 during the monsoons when $\hat{h}_1$ is thick, and as a result the daily-averaged phytoplankton growth rate (proportional to curve $\overline{\mathcal{I}_1\mathcal{N}_1}$) is increased as well. The P_1 levels, however, are not larger in solution 3 than solution 2 during the monsoons but actually are slightly lower (Figures 3 and 4a). Thus the growth rate increase does not significantly raise production in the model, contrary to the hypothesis proposed in the introduction. The reason it does not is because the increase in P_1 due to the larger growth rate is more than balanced by a decrease in P_1 during nighttime entrainment. The resulting lower P_1 values contribute significantly to the increased N_1 levels during the monsoons.

The most striking property of the $\overline{\mathcal{I}_1}$ fields, however, is the marked weakening of $\overline{\mathcal{I}_1}$ in solution 3 during the intermonsoon periods. This happens because h_1 is thin enough throughout its daily cycle for $\mathcal{I}_1$ always to be nearly saturated (i.e., always close to 1). Thus $\mathcal{I}_1$ does not increase enough in the day when h_1 thins to compensate for the lack of light during the night, and $\overline{\mathcal{I}_1}$ decreases by a factor of about 2. Despite this decrease, $\overline{\mathcal{I}_1\mathcal{N}_1}$ is still larger in solution 3 because $\overline{\mathcal{N}_1}$ increases by a factor of about 3, owing to the thicker $\hat{h}_1$ and hence increased entrainment.

3.1.3.2. Diurnal pumping: There is an inherent vertical mixing process in the model driven by the diurnal cycling of h_1. It can happen in two ways. The first type (type 1) occurs at the end of the monsoons when the daily minimum of h_2, $\check{h}_2$, is thicker than $h_{2\min}$, as in the right-hand portion of Figure 4b. When h_1 thins during any day, detrained layer 1 variables q_1 are necessarily mixed into layer 2, since only the average value in the layer q_2 can be retained; consequently, during the following night the values of q_2 that are entrained back into the mixed layer generally differ from the q_1 values detrained the previous day. The second type (type 2) occurs when $\check{h}_2 = h_{2\min}$, as in the left-hand portion of Figure 4b. Depending on the value of $\hat{h}_1'$, w_d typically changes $h_1 + h_2$ by a small amount during the day. If it thickens $h_1 + h_2$, q_3 variables are entrained into layer 2 during the day. If it thins $h_1 + h_2$, then when h_1 approaches $\hat{h}_1$ the following night, q_3 values are first entrained into layer 2 and then into layer 1. In both types, subsurface variables are mixed upward into layer 1, a process we refer to as "diurnal pumping."

With the choice for $\hat{h}_1'$ in (4b), type 2 diurnal pumping is essentially eliminated in the model, as indicated in Figure 4b by $h_1 + h_2$ being almost flat between h_1 peaks during the first half of February. (In fact, $h_1 + h_2$ rises slightly between peaks, but the rise is due to mass convergence rather than w_d.) Type 1 diurnal pumping affects the physical model during the intermonsoon seasons by mixing subsurface temperatures into layer 1 and hence lowering T_1 by 0.5°–0.75°C. It affects the biological model by keeping N_1 levels higher after the end of the monsoons, thereby strengthening, broadening, and delaying the peaks of the spring and fall blooms.

It should be noted that diurnal pumping in our model is not a well-defined physical process, but rather happens "artificially" because the model's low resolution requires that detrained variables are mixed throughout subsurface layers. Indeed, we introduced the diurnal thermocline layer to minimize this mixing, allowing the system to "remember" variables more faithfully throughout the diurnal cycle. (In our original solutions without the diurnal thermocline layer, seasonal thermocline variables are continually mixed upward into layer 1; as a result, h_1 thickens 2–3 weeks earlier than in solution 3, and the spring, fall, and intermonsoon blooms are 1½–2 times stronger.) There are indications, however, that sub-mixed-layer mixing does occur at the mooring site: After the mixed layer thins during the day, turbulence (indicated by a localized region of enhanced current shear) sometimes extends downward into the seasonal thermocline (A. S. Fischer et al., Mesoscale eddies, coastal upwelling, and the upper-ocean heat budget in the Arabian Sea, submitted to *Deep-Sea Research*, 2001, hereinafter referred to as Fischer et al., submitted manuscript, 2001), in a manner reminiscent of the daily penetration of turbulence into the equatorial thermocline [*Brainerd and Gregg*, 1995; *Lien et al.*, 1995]. In addition, diurnal pumping also occurs in other types of mixed-layer models with much higher vertical resolution [*Fischer*, 2000]. At the present time, however, sub-mixed-layer mixing is not well enough understood to be properly represented in ocean models.

The potential importance of diurnal pumping in biological processes has been discussed previously by *Gardner et al.* [1995, 1999]. Among other things, the authors note that if the nutricline is shallower than the daily maximum of h_m, $\hat{h}_m$, then diurnal cycling of h_m can pump nutrients into the euphotic zone. They did not, however, comment on the processes that are required to maintain a nutricline shallower than h_m, which must involve sub-mixed-layer mixing or possibly horizontal advection.

3.2. Daily Forcing

3.2.1. Solution without diurnal forcing. Figure 6 shows the solution forced by daily fields without diurnal forcing (solution 4). The overall annual structure of h_1 is similar to that of its climatological counterpart (solution 2, Figure 3) but with pulses of thinner h_1 near the ends of both monsoons associated with break periods when P_r in (3b) becomes negative. There are also pulses of thicker h_1 during the intermonsoon periods generated by wind events. The spring bloom is now divided into four distinct peaks, each of which is a detrainment bloom associated with a period when h_1 thins to be close to $h_{1\min}$ for a week or more. (The thinning event during mid-January only caused a weak P_1 response because h_1 did not become thin enough or was too short.) As a consequence, the overall spring bloom

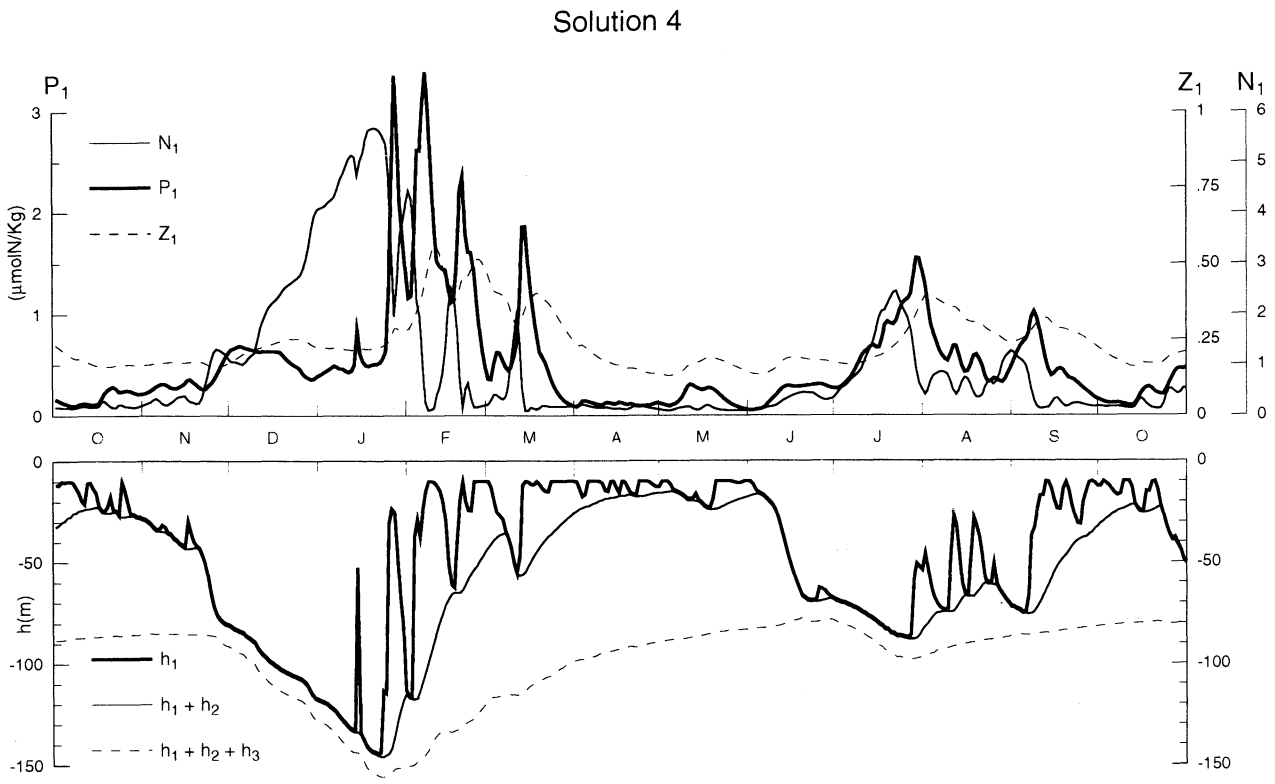

Figure 6. As in Figure 3, except for the solution forced by daily winds without diurnal forcing (solution 4). The spring and fall blooms are split into a series of detrainment blooms associated with monsoon breaks.

lasts much longer, extending from the end of January until mid-March. Note that the individual bloom events rapidly deplete the nutrient supply N_1, but it is quickly replenished by subsequent entrainment. Similarly, the fall bloom now consists of two events, caused by a break of several weeks' duration during August. Interestingly, they are a combination of entrainment and detrainment blooms: Each begins with a gradual increase in P_1 due to entrainment of N_1 and ends with a pulse of P_1 due to a detrainment event. Three other noteworthy blooms occur in December, May and June, each generated by prominent entraining events.

3.2.2. Solution with diurnal forcing. Figure 7a shows the solution forced by daily fields with diurnal forcing (solution 5). Generally, the response is similar to that of solution 4 (Figure 6), and differences between solutions 4 and 5 are similar to those between solutions 2 and 3. Most notably, at the end of the northeast monsoon $\hat{h}_1$ remains thicker longer than h_1 does in solution 4, and this difference affects the spring bloom by altering the timing and strength of individual peaks. Indeed, the first large peak in solution 4 (at the end of January) is absent in solution 5 because $\hat{h}_1$ does not thin much at all, and the final one is broader. As a result, the overall spring bloom in solution 5 is delayed by 2–3 weeks relative to solution 4. In addition, N_1 values are higher throughout the year, and P_1 levels are higher during the intermonsoon seasons, including the May and October/November blooms, and lower during the monsoons. These differences appear to have the same dynamical causes that they do in the climatological solutions, although this interpretation is less clear owing to the strong intraseasonal variability.

3.3. Comparison With Observations

3.3.1. Mixed layer. For comparison with the h_m field in Figure 1, Figure 7b plots instantaneous values of h_1 from solution 5 throughout the year (top panel) and during February (bottom panel). The h_1 response is strikingly similar to that of h_m in Figure 1, with most of the intraseasonal pulses of h_m being captured by $\hat{h}_1$. This agreement generally holds for their daily maxima and minima so that even the amplitude variability of the diurnal cycle is well represented in solution 5. Note, for example, that during the northeast monsoon there are several pulses when the diurnal cycle is small or absent, and that similar weak amplitude events are present in h_m. They are due to strong wind events that increase $\mathcal{W}$ and hence h_{mo}. Moreover, even the structures of the diurnal cycle are similar, with modeled and observed fields typically thinning rapidly during the day and thickening somewhat less quickly during the night (compare bottom panels of Figures 1 and 7b).

Two prominent differences between the thicknesses

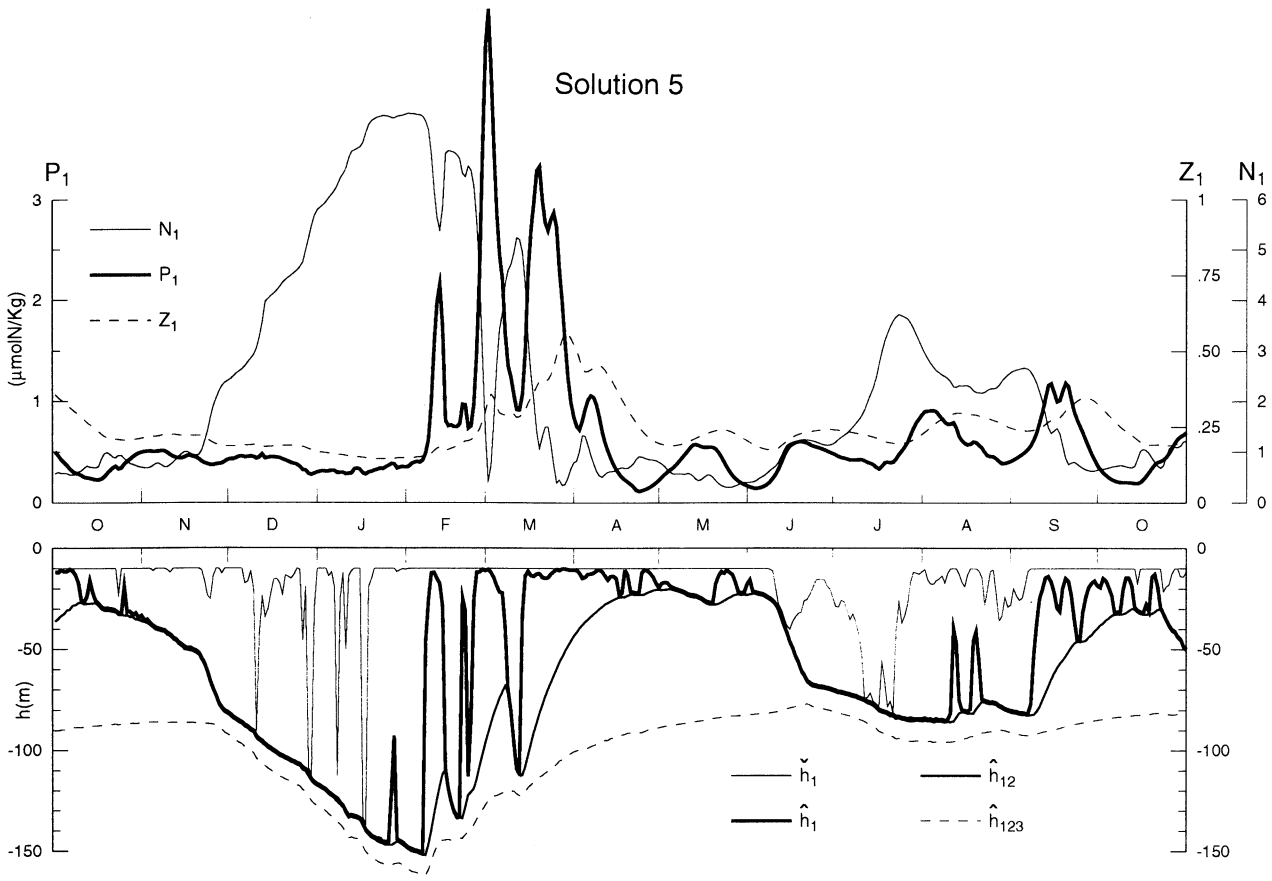

Figure 7a. As in Figure 4a, except for the solution forced by daily winds with diurnal forcing (solution 5). In comparison with solution 4, the spring bloom is delayed by 2 3 weeks, and the summer and fall blooms are weaker.

are that h_m shallows at the end of November 1994 and during August 1995 but h_1 does not (top panels of Figures 1 and 7b); these differences are likely due to the passage of two eddies through the mooring area that are not present in solution 4 (Fischer et al., submitted manuscript, 2001). Other noteworthy differences are that $\hat{h}_1$ is considerably less than $\hat{h}_m$ at the end of the winter monsoon and for the February and March spikes. The cause of these discrepancies is not clear: It could result from deficiencies in the parametrization of w_k, from the model underestimating $\Delta\rho'$, from errors in estimating h_m by temperature data alone, or from the finite vertical separation of the mooring sensors (25 m below 100 m).

3.3.2. Biology. Figures 8a and 8b plot daily-averaged phytoplankton biomass $\mathcal{B}_i = \sum_{j=1}^{i} \overline{h_j P_j}$ and production $\mathcal{P}_i = \sum_{j=1}^{i} g_p \overline{h_j \mathcal{I}_j \mathcal{N}_j P_j}$, respectively, showing values in layer 1 ($\mathcal{B}_1$ and $\mathcal{P}_1$, thin curves), in layers 1+2 ($\mathcal{B}_2$ and $\mathcal{P}_2$, light shading), and in layers 1+2+3 ($\mathcal{B}_3$ and $\mathcal{P}_3$, heavy shading). Because corresponding sets of curves for biomass and production are so similar, Figure 8b only includes curves for solution 5. The panels also include estimates of total biomass $\mathcal{B}_m$ and productivity $\mathcal{P}_m$ (thick curves), determined from the mooring bio-optical sensors by *Marra et al.* [1998]. Values of $\mathcal{B}_i$ are converted to chlorophyll concentrations (mg/m^3) assuming a C:Chl *a* ratio of 80:1 (wt:wt), and $\mathcal{P}_i$ values are converted to carbon units (mmol C m^{-2} d^{-1}). Both conversions assume Redfield stoichiometry.

Generally, observed and modeled biomass fields compare most favorably for solution 5, both having about the same amplitude and similar annual cycles: Biomass is higher during the monsoon seasons, lower during the intermonsoons (for $\mathcal{B}_2$ but not $\mathcal{B}_3$), and the spring bloom peaks in late February. There are also general disagreements, which as discussed next may be related to observational errors or model deficiencies.

During the monsoons, solution 5's biomass $\mathcal{B}_3$ is somewhat larger than the observed biomass $\mathcal{B}_m$. A possible cause of this discrepancy is fouling of the mooring's optical sensors. As a result, there was no optical data above 65 m from mid-January through April and above 35 m from mid-July through the end of the observation period, and occasional shipboard profiles had to be used to help fill in these time series gaps (plus signs in Figures 8a and 8b [*Marra et al.*, 1998; *Dickey et al.*, 1998]). Thus the strength of the near-surface biomass was likely underestimated at these times.

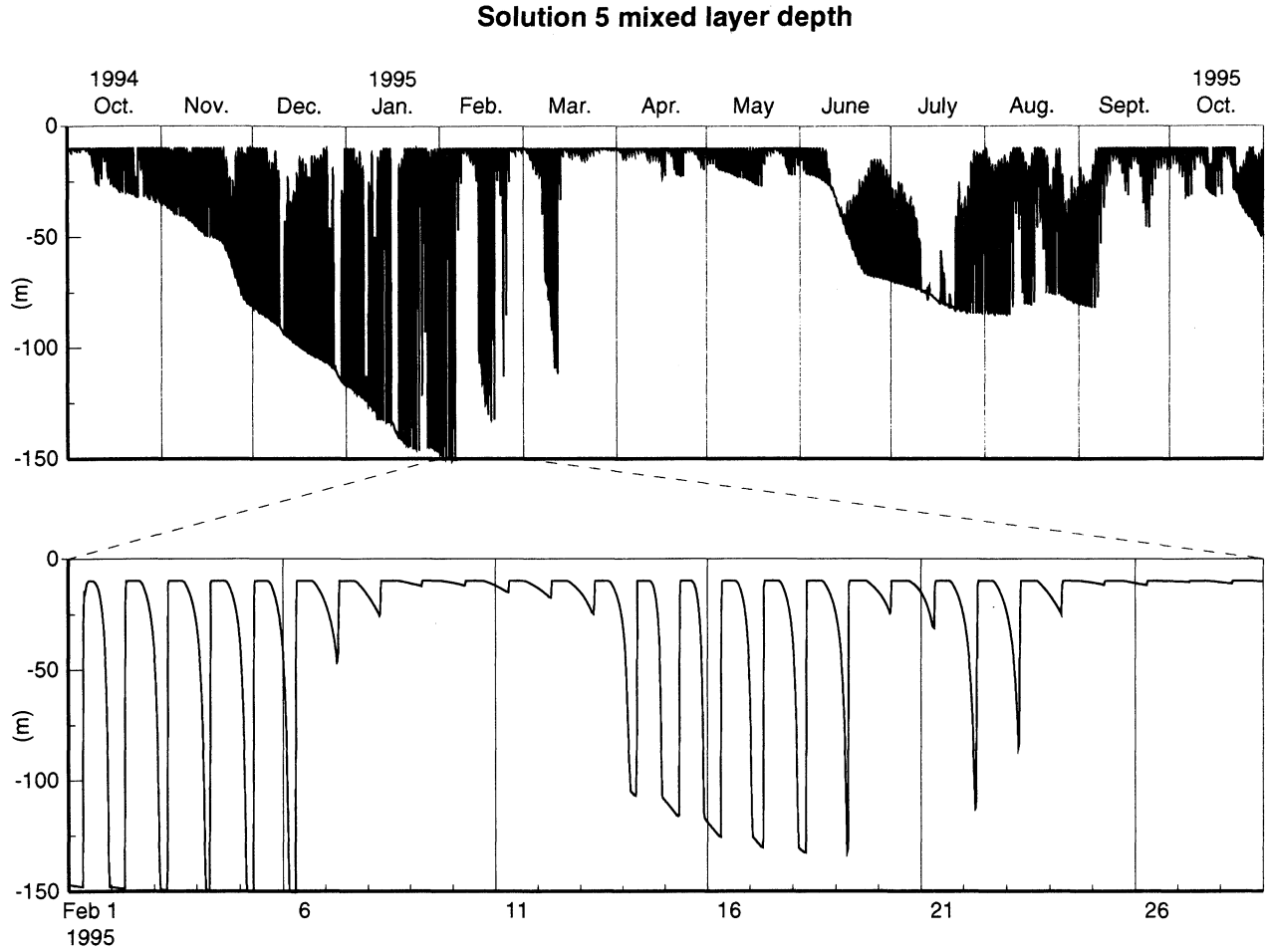

Figure 7b. Similar to Figure 1, except showing mixed-layer thickness h_1 from solution 5.

During the summer intermonsoon, $\mathcal{B}_3$ is considerably larger than $\mathcal{B}_m$ in all the solutions except solution 1. At these times, $h_1 + h_2$ is thin and layer 3 is therefore close to the surface. A possible cause of this difference, then, is that with $I_o = 40$ W/m^2 there is too much phytoplankton growth in layer 3 (as measured by $\mathcal{P}_3 - \mathcal{P}_2$ and $\mathcal{B}_3 - \mathcal{B}_2$). Indeed, with $I_o = 100$ W/m^2 (solution 1) production and biomass in layer 3 are much lower, and $\mathcal{B}_3$ is closer to the observations (top panel of Figure 8a). On the other hand, another possible cause is that $\mathcal{B}_m$ is again underestimated by the mooring optical sensors. There was an intense band of high chlorophyll concentrations confined almost entirely between 25 m and 65 m with a maximum near 40 m during the intermonsoon [*Gundersen et al.*, 1998; *Gardner et al.*, 1999]. The mooring sensors (at 10 m, 35 m, and 65 m) appear to have missed most of this signal.

There are two occasions in solution 5 when $\mathcal{B}_m$ is larger than $\mathcal{B}_3$ (and $\mathcal{P}_m$ is larger than $\mathcal{P}_3$). The first instance is the short-lived intense bloom in December. As was noted above, at this time an eddy passed the mooring site that thinned h_m (compare Figures 1 and 7b). It is likely that the bloom resulted from this thinning, or possibly from the advection of nutrients into the region by the eddy. The second instance is in late September and October, when $\mathcal{B}_3$ drops markedly but $\mathcal{B}_m$ does not. The cause of this discrepancy is not clear. It may be related to the passage of the second eddy during August, which also caused h_m to thin significantly; however, in contrast to the December case, this thinning apparently did not cause an intense detrainment bloom. Fouling might also account for the larger $\mathcal{B}_m$ values in October, if there was a sharp decline in the near-surface biomass that was missed owing to the lack of data above 35 m.

4. Summary and Discussion

In this study, we use a coupled, physical-biological model to assess the influence of diurnal and intraseasonal forcing on mixed-layer thickness and biological variability in the central Arabian Sea throughout the year. In addition, we report on the sensitivity of solutions to the specification of the phytoplankton light response function $\mathcal{I}_i$. The physical model is a $4^1/_2$-layer system, in which entrainment into, and detrainment from, layer 1 (the surface mixed layer) is determined primarily by *Kraus and Turner* [1967] physics

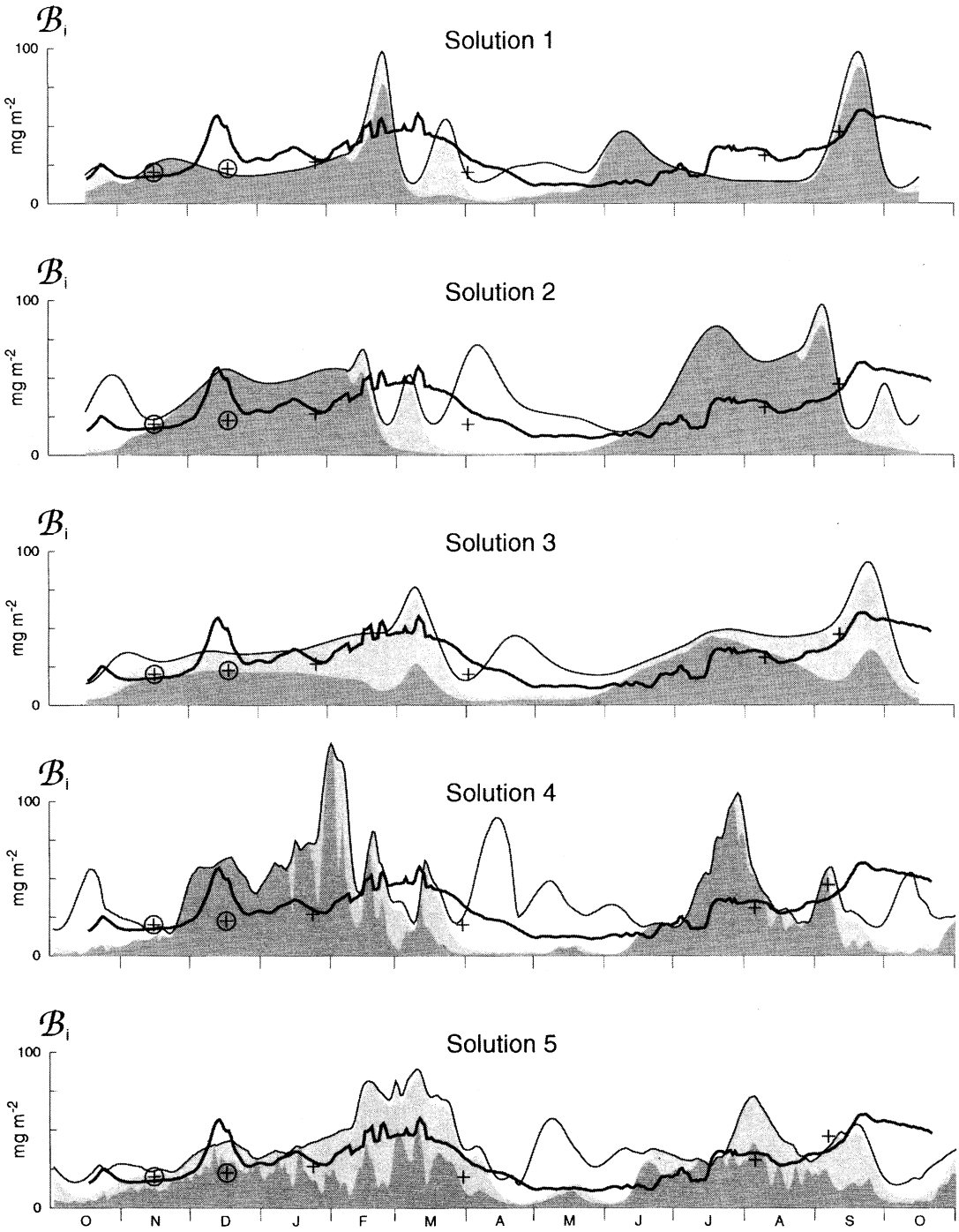

Figure 8a. Time plots of biomass for solutions 1 5 showing $\mathcal{B}_3$ (thin curve), $\mathcal{B}_2$ (light shading), and $\mathcal{B}_1$ (heavy shading). Each panel also includes a plot of biomass estimated from the mooring data $\mathcal{B}_m$ (thick curve). The plus signs indicate values obtained near the mooring site during six cruises; the circled plus signs are from cruises taken the following year, that is, during November and December of 1995.

(section 2.1). The biological model is the same as the MKHO system, differing only in the value of I_o (section 2.2). Both monthly climatological and daily fields are used to drive the model, and diurnal forcing is included by allowing the incoming solar radiation to have a daily cycle (section 2.3).

The climatological solution with $I_o = 100$ W/m^2 and without diurnal forcing (solution 1) has two major blooms in the spring and fall (top panel of Figure 3). They are detrainment blooms that happen when the mixed layer thins and $\mathcal{I}_1$ is increased. In comparison with observed values, N_1 levels are unrealistically high

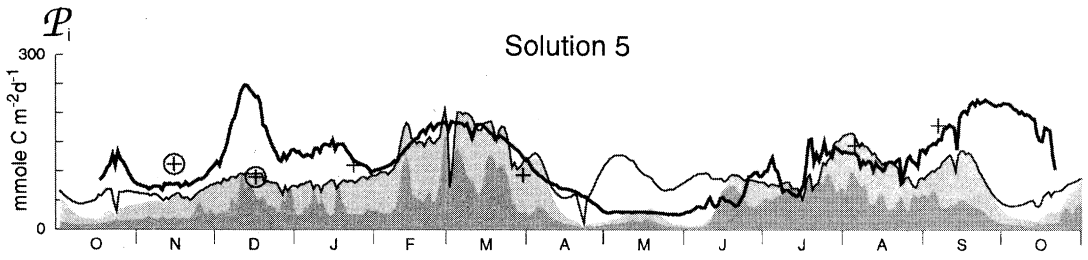

Figure 8b. Time plots of production, showing $\mathcal{P}_3$ (thin curve), $\mathcal{P}_2$ (light shading), and $\mathcal{P}_1$ (heavy shading) for solution 5, $\mathcal{P}_m$ (thick curve) estimated from the mooring data, and point values obtained during six cruises (for symbols see the caption to Figure 8a).

during the monsoons, the spring and fall blooms are too short-lived and intense, and there is no summertime bloom. When I_o is reduced to 40 W/m^2 (solution 2), P_1 levels increase and N_1 levels drop to reasonable values during the monsoons, and the spring and fall blooms are much less intense (middle panel of Figure 3). In the climatological solution with diurnal forcing (solution 3), the spring and fall blooms are broader, stronger, and delayed by about 3 weeks (Figure 4a).

Diurnal cycling of h_1 affects the climatological solutions in two basic ways. First, it increases $\overline{\mathcal{I}_1}$ during the monsoons when $\hat{h}_1$ is thick and, owing to light saturation, weakens it by a factor of 2 during the intermonsoons when $\hat{h}_1$ is thin (Figure 5). In the former case, the resulting increase in growth rate $g_p\overline{\mathcal{I}_1\mathcal{N}_1}$ does not cause an increase in P_1 because of downward mixing during nighttime entrainment. In the latter, the weakened $\overline{\mathcal{I}_1}$ is more than compensated for by an increase in $\overline{\mathcal{N}}_1$, strengthening the growth rate and increasing P_1 levels (section 3.1.3.1). Second, the diurnal cycling of h_1 enhances vertical exchange of variables between the mixed and subsurface layers in the model (section 3.1.3.2). With the choice of $\hat{h}_1'$ in equation (4a), however, this diurnal pumping process affects the model only after the end of the monsoons when $\hat{h}_1$ separates from $h_1 + h_2$ (type 1 pumping). It increases N_1 values at these times, thereby strengthening, broadening, and delaying the spring and fall blooms. There are in fact indications of enhanced mixing just below $\hat{h}_m$ at the mooring site and in other mixed-layer models as well [*Fischer*, 2000]. In our model, however, it is not a well-defined physical process but rather happens because of the model's limited vertical resolution, since detrained variables are necessarily mixed throughout subsurface layers.

In the daily solution without diurnal forcing (solution 4), the overall spring bloom is much broader, being split into a series of detrainment blooms when h_1 thins during monsoon break periods, and the fall bloom is split into two parts (summer and fall blooms) by a break during August (Figure 6). In the daily solution with diurnal forcing (solution 5), the spring bloom is delayed by 2–3 weeks and the summer and fall blooms are weaker and delayed. These changes are similar to those for the climatological solutions and likely happen for the same dynamical reasons.

Among the solutions, solution 5 compares best with estimates of mixed-layer thickness h_m, phytoplankton biomass $\mathcal{B}_m$, and phytoplankton production $\mathcal{P}_m$ fields determined from mooring observations (Figures 1, 7a, 8a, and 8b). The h_m and h_1 fields compare remarkably well, differing considerably only in December and August, when eddies passed the mooring site. The overall annual cycles of biomass and production also compare favorably. Differences are potentially due to the growth rate of the model phytoplankton being too large under low-light conditions, fouling of near-surface mooring sensors during the monsoons, the presence of a subsurface chlorophyll maximum during the summer intermonsoon undetected by the mooring sensors, and the passage of two eddies across the mooring site.

It is noteworthy that both the observed and modeled phytoplankton biomass and production (Figures 8a and 8b) vary seasonally by less than a factor of 10. This relatively low amplitude variability happens in the model because h_1 and h_m do not thicken too much (<150 m) during either of the monsoons. As a result, phytoplankton growth in the central Arabian Sea continues to some degree during deep-mixing periods, which in turn tends to damp detrainment blooms associated with the relaxation of the winds. In contrast, variations in P_1 are much more pronounced (spiky) than those of $\mathcal{B}_3$. Thus assessments of seasonal variability using satellite chlorophyll measurements [e.g., *Banse*, 1994; *Banse and English*, 1999] may tend to underestimate the strength of the blooms associated with the monsoons because they only sample the surface waters.

In conclusion, perhaps our most important result is the demonstration that higher-frequency (diurnal and intraseasonal) forcing is a potentially important aspect of Arabian Sea biological and mixed-layer dynamics. The duration, timing, strength, and episodicity of blooms differ markedly among our solutions, and these differences cannot be simply characterized as noise superimposed upon a smooth climatological signal. Rather, they result from highly nonlinear physical

and biological processes (e.g., the influences of the diurnal cycle of h_1 and $\mathcal{I}_1$ and of diurnal pumping on T_1 and N_1). Another noteworthy result is that the model's biological activity is primarily determined by the local structure of h_1, that is, the biological response is largely one dimensional. (We quantified this result in two test solutions comparable to solution 5: one without advection terms in any of the biological variables and another with advection only on N. The structures of $NPZD$ curves were unchanged in both tests, but their amplitudes decreased by about 15% in the first and 5% in the second. Thus advection influences the biological response nearly an order of magnitude less than local processes do.) The lack of substantial three-dimensional effects may be fortuitous, however, a consequence of the passage of only two prominent eddies past the mooring site. Finally, our study focuses attention on the importance of sub-mixed-layer mixing processes, suggesting that only when they are understood and properly parameterized can effects of diurnal forcing be properly simulated in ocean models.

We caution that these conclusions are based on a specific coupled model, with coarse vertical resolution and a very simple biological component. It is reasonable then to question their generality. In particular, the sensitivity of solutions to diurnal forcing is, to some degree, a result of the model's low vertical resolution: Layer (and level) models with increased vertical resolution should be less sensitive to the effects of diurnal forcing because they resolve sub-mixed-layer mixing processes better. In addition, a key aspect of the biological model is the sensitivity of the phytoplankton growth rate $g_P\mathcal{N}_1\mathcal{I}_1$ to mixed-layer thickness through its influence on $\mathcal{I}_1$. This sensitivity may be weaker in more complex biological models, for example, in a system with several types of phytoplankton having a range of I_o values or one that allows for photoadaptive changes in I_o. Despite its limitations, we believe that the processes active in our model are basic ones that are also present in better resolved and more complex systems. Moreover, given the constraints imposed by computational speed, poor spatial resolution and limited biological complexity in biophysical models are issues that will have to be dealt with for some time to come.

Acknowledgments. This research was sponsored by the Office of Naval Research through grants N00014-97-1-0077 and N00014-94-1-0161 and by the National Science Foundation through grant OCE-9818708. J.P.M. acknowledges support from the Frontier Research System for Global Change through its sponsorship of the IPRC. A.S.F. was also supported through the ONR Secretary of the Navy Chair awarded to R.A.W. We thank John Marra, Chris Kinkade, and Cheng Ho for providing their chlorophyll and primary productivity estimates for comparison with our model results; Tom Dickey and John Marra for velocity, temperature, and conductivity data from their mooring instruments (MVMSs); Weiqing Han for her assistance in the development of our mixed-layer code; and Richard Barber for helpful discussions. This manuscript is JGOFS Contribution 586, SOEST Contribution 5324, IPRC Contribution 72, and WHOI Contribution 10181.

References

Banse, K., Seasonality of phytoplankton chlorophyll in the central and northern Arabian Sea, *Deep Sea Res., Part A, 34*, 713–723, 1987.

Banse, K., On the coupling of hydrography, phytoplankton, zooplankton, and settling organic particles offshore in the Arabian Sea, *Proc. Indian Acad. Sci. Earth Planet. Sci., 103*, 125–161, 1994.

Banse, K., and D. C. English, Geographical differences in seasonality of CZCS-derived phytoplankton pigment in the Arabian Sea for 1978-1986, *Deep-Sea Res., Part II, 47*, 1623–1677, 2000.

Brainerd, K. E., and M. C. Gregg, Surface mixed and mixing layer depths, *Deep Sea Res., Part II, 42*, 1521–1543, 1995.

Dickey, T., J. Marra, D. E. Sigurdson, R. A. Weller, C. S. Kinkade, S. E. Zedler, J. D. Wiggert, and C. Langdon, Seasonal variability of bio-optical and physical properties in the Arabian Sea: October 1994-October 1995, *Deep Sea Res., Part II, 45*, 2001–2025, 1998.

Fasham, M. J. R., H. W. Ducklow, and S. M. McKelvie, A nitrogen-based model of plankton dynamics in the oceanic mixed layer, *J. Mar. Res., 48*, 591–639, 1990.

Fischer, A. S., The upper ocean response to the monsoon in the Arabian Sea, Ph.D. thesis, Mass. Inst. of Technol./Woods Hole Oceanogr. Inst., Woods Hole, Mass., 2000.

Gardner, W. D., S.-P. Chung, M. J. Richardson, and I. D. Walsh, The oceanic mixed-layer pump, *Deep Sea Res., Part II, 42*, 757–775, 1995.

Gardner, W. D., J. S. Gundersen, M. J. Richardson, and I. D. Walsh, The role of seasonal and diel changes in mixed-layer depth on carbon and chlorophyll distributions in the Arabian Sea, *Deep Sea Res., Part II, 46*, 1833–1858, 1999.

Gundersen, J. S., W. D. Gardner, M. J. Richardson, and I. D. Walsh, Effects of monsoons on the seasonal and spatial distributions of POC and chlorophyll in the Arabian Sea, *Deep Sea Res., Part II, 45*, 2103–2132, 1998.

Han, W., Influence of salinity on dynamics, thermodynamics and mixed-layer physics in the Indian Ocean, Ph.D. thesis, 147 pp., Nova Southeastern Univ., Fort Lauderdale, Fla., 1999.

Han, W., J. P. McCreary, D. L. T. Anderson, and A. J. Mariano, Dynamics of the eastern surface jets in the equatorial Indian Ocean, *J. Phys. Oceanogr., 29*, 2191–2209, 1999.

Kraus, E. B., and J. S. Turner, A one-dimensional model of the seasonal thermocline. II: The general theory and its consequences, *Tellus, 119*, 98–106, 1967.

Legates D. R., and C. J. Willmott, Mean seasonal and spatial variability in gauge-corrected global precipitation, *Intl. J. Climatology, 10*, 111–127, 1990.

Legler, D. M., I. M. Navon, and J. J. O'Brien, Objective analysis of pseudo-stress over the Indian Ocean using a direct-minimization approach, *Mon. Wea. Rev., 117*, 709–720, 1989.

Leonard, C. L., C. R. McClain, R. Murtugudde, E. E. Hoffman, and L. W. Harding Jr., An iron-based ecosystem model of the central equatorial Pacific, *J. Geophys. Res., 104*, 1325–1341, 1999.

Levitus, S., R. Burgett, and T. P. Boyer, *World Ocean Atlas 1994*, vol. 3, *Salinity, NOAA Atlas NESDIS*, vol. 3, 111 pp., Natl. Oceanic and Atmos. Admin., Silver Spring, Md., 1994.

Lien, R.-C., D. R. Caldwell, M. C. Gregg, and J. N. Moum, Turbulence variability at the equator in the central Pacific

at the beginning of the 1991–1993 El Niño, *J. Geophys. Res.*, *100*, 6881–6898, 1995.

Marra, J., T. D. Dickey, C. Ho, C. S. Kinkade, D. E. Sigurdson, R. A. Weller, and R. T. Barber, Variability in primary production as observed from moored sensors in the central Arabian Sea in 1995, *Deep Sea Res., Part II*, *45*, 2253–2267, 1998.

McCreary, J. P., and P. K. Kundu, A numerical investigation of sea-surface temperature variability in the Arabian Sea, *J. Geophys. Res.*, *94*, 16,097–16114, 1989.

McCreary, J. P., P. K. Kundu, and R. L. Molinari, A numerical investigation of the dynamics, thermodynamics and mixed-layer physics in the Indian Ocean, *Prog. Oceanogr.*, *31*, 181–244, 1993.

McCreary, J. P., K. E. Kohler, R. R. Hood, and D. B. Olson, A four-component ecosystem model of biological activity in the Arabian Sea. *Prog. Oceanogr.*, *37*, 117–165, 1996.

Morel, A., and D. Antoine, Heating rate within the upper ocean in relation to its bio-optical state, *J. Phys. Oceanogr.*, *24*, 1652–1665, 1994.

Morrison, J. M., L. A. Codispoti, S. Gaurin, B. Jones, V. Manghnani, and Z. Sheng, Seasonal variation of hydrographic and nutrient fields during the US JGOFS Arabian Sea Process Study, *Deep Sea Res., Part II*, *45*, 2053–2101, 1998.

Paulson, C. A., and J. J. Simpson, Irradiance measurements in the upper ocean, *J. Phys. Oceanogr.*, *7*, 952–956, 1977.

Price, J. F., R. A. Weller, and R. Pinkel, Diurnal cycling, Observations and models of the upper ocean response to diurnal heating, cooling, and wind mixing, *J. Geophys. Res.*, *91*, 8411–8427, 1986.

Rao, R. R., R. L. Molinari, and J. F. Festa, Evolution of the climatological near-surface thermal structure of the tropical Indian Ocean, 1, Description of mean monthly mixed layer depth and sea surface temperature, surface current, and surface meteorological fields, *J. Geophys. Res.*, *94*, 10,801–10,815, 1989.

Rao, R. R., R. L. Molinari, and J. F. Festa, Surface meteorological and near surface oceanographic atlas of the tropical Indian Ocean, *NOAA Tech. Memo. ERL AOML-69*, 59 pp., NOAA Environ. Res. Lab., Boulder, Colo., 1991.

Weller, R. A., M. F. Baumgartner, S. A. Josey, A. S. Fischer, and J. C. Kindle, Atmospheric forcing in the Arabian Sea during 1994–1995: observation and comparisons with climatology and models, *Deep Sea Res., Part II*, *45*, 1961–1999, 1998.

A. S. Fischer and R. A. Weller, Woods Hole Oceanographic Institution, Woods Hole, MA 02543. (afischer@typhoon.whoi.edu; rweller@whoi.edu)

R. R. Hood, University of Maryland Center for Environmental Science, Cambridge, MD 21613. (raleigh@hpl.umces.edu)

J. Kindle, Naval Research Laboratory, Stennis Space Center, MS 39529. (kindle@nrlssc.navy.mil)

K. E. Kohler, Oceanographic Center, Nova Southeastern University, Dania, FL 33004. (kevin@nova.edu)

J. P. McCreary, International Pacific Research Center, School of Ocean and Earth Science and Technology, University of Hawaii, 2525 Correa Road, Honolulu, HI 96822. (jay@iprc.soest.hawaii.edu)

S. Smith, Rosenstiel School of Marine and Atmospheric Science, Miami, FL 33149. (ssmith@rsmas.miami.edu)

(Received December 14, 1999; revised September 21, 2000; accepted October 19, 2000.)